**Smart Structures and Systems**, *Vol. 14, No. 5 (2014) 743-763*
DOI: http://dx.doi.org/10.12989/sss.2014.14.5.743 

# Period doubling of the nonlinear dynamical system of an electrostatically actuated micro-cantilever

Y.M. Chen* and J.K. Liu[a]

*Department of Mechanics, Sun Yat-sen University, 135 Xingang Road, Guangzhou 510275, China*

*(Received July 14, 2012, Revised August 14, 2013, Accepted August 31, 2013)*

**Abstract.** The paper presents an investigation of the nonlinear dynamical system of an electrostatically actuated micro-cantilever by the incremental harmonic balance (IHB) method. An efficient approach is proposed to tackle the difficulty in expanding the nonlinear terms into truncated Fourier series. With the help of this approach, periodic and multi-periodic solutions are obtained by the IHB method. Numerical examples show that the IHB solutions, provided as many as harmonics are taken into account, are in excellent agreement with numerical results. In addition, an iterative algorithm is suggested to accurately determine period doubling bifurcation points. The route to chaos via period doublings starting from the period-1 or period-3 solution are analyzed according to the Floquet and the Feigenbaum theories.

**Keywords:** micro-cantilever; incremental harmonic balance method; Floquet theory; period doubling; chao

## 1. Introduction

Most micro-electro-mechanical (MEMS) inherently contains nonlinearities, such as intrinsic and exterior nonlinearities arising from coupling of different domains (Senturia 1998, Lyshevski 1997). Also, there exist mechanical nonlinearities, i.e., large deformations, surface contact, creep phenomena, time-dependent masses and nonlinear damping effects (De and Aluru 2006, Ashhab *et al*. 1999), etc. Effective nonlinear dynamic analysis becomes an increasingly important task in MEMS research and manufacturing.

The nonlinear dynamical behaviors of micro-cantilever based instrument in MEMS under various loading conditions have stimulated the curiosities and interests of many researchers (Passiana *et al*. 2003, Manna *et al*. 2010, Chan *et al*. 2000, Mahmoodi and Jalili 2009, Fu and Zhang 2009). For instance, the nonlinear vibrations of an electrostatically actuated micro-cantilever based device in MEMS were investigated through a simplified mass-spring-damping model subjected to nonlinear electrostatic force (Liu *et al*. 2003 and 2004, Zhang *et al*. 2007). The computation of the nonlinear dynamical systems of a micro-cantilever or other micro-structures focuses on using numerical methods (Meng *et al*. 2009). Since complicated nonlinearities exist in the governing equations of motions of the electrostatically actuated

*Corresponding author, E-mail: chenyanmao@hotmail.com
[a] Professor, E-mail: jikeliu@hotmail.com


http://www.techno-press.org/?journal=sss&subpage=8 ISSN: 1738-1584 (Print), 1738-1991 (Online)

micro-cantilever, Zhang and Meng (2005) suggested an approximate approach via expanding the nonlinearities into Taylor series and retaining only the first one and/or two terms. The simplified series of the nonlinear terms make it possible to implement harmonic balancing process. This process is the main procedure of harmonic balance method. Essentially, it equates the coefficient of each harmonic to zero hence a series of algebraic equations can be deduced. Also based on this simplification, Chen *et al*. (2010) proposed an iteration algorithm to analyze the periodic solutions.

Numerical analysis shows that nonlinear MEMS systems can exhibit a lot of complex dynamical behaviors, such as period doubling bifurcations, sub-harmonic responses and chaos. The period doublings and symmetry breakings of MEMS systems have been investigated by many researchers based on experimental as well as simulation results (Nayfeh and Younis 2005). De and Aluru (2006) investigated the period doubling bifurcation of an electrostatically actuated microstructures by using time marching integration. Also using numerical method, Najar *et al*. (2010a, b) found that the nonlinear system of an electrostatic microactuator may exhibit period doublings when the excitation frequency locates in the resonance region. Towfighian *et al*. (2011) investigated the closed-loop dynamics of an electrostatic micro-beam, and analyzed the period doublings and reverse period doublings when the excitation frequency and amplitude sweep. Period doublings were also observed in nano-scale microsystems such as atomic force microscopy (Hu and Raman 2006).

The subharmonic responses after period doublings are generally solved by numerical techniques. Well-known, numerical approaches such the Runge-Kutta method can only trace stable solutions. On the other hand, unstable solutions especially periodic ones are useful to better understanding of nonlinear dynamical behaviors such as bifurcations and routes to chaos. It is necessary to propose some analytical or semi-analytical techniques to efficiently detect both stable and unstable periodic solutions.

Predicting nonlinear dynamic responses for scientific and engineering problems has been an active field for many years (Bayat and Pakar 2012, Borzi *et al*. 2013, and Waris and Ishihara 2012). Many approaches, both analytical and numerical types, were developed. Among various methods for nonlinear dynamics analysis, there is a widely-used semi-analytical approach named incremental harmonic balance (IHB) method. The IHB method was initiated in 1980s by Lau and Cheung (1981). This method has many advantages over other techniques. It can be applied to deal with strongly nonlinear systems and provides highly accurate results. Moreover, it is a much simpler and more systematic approach and consequently can be more easily implemented on a computer than the perturbation method. The IHB method is indeed exactly equivalent to the harmonic balance (HB) plus the Newton Raphson method (Ferri 1986). The IHB method has been successfully applied to the analysis of many periodic and almost periodic vibration and related problems (Raghothama and Narayanan 1999, Xu *et al*. 2003, Shen *et al*. 2008).

The major motivation of this study is to employ the IHB method to analyze the dynamical behaviors of an electrically actuated micro-cantilever. In the solution procedure of the IHB method, an inevitable step is to expand the incremental equations as truncated Fourier series. As shown later, it is very cumbersome to realize this step because the electrostatic force is expressed as a fractional function. It is sometimes impossible to implement some routine procedures to complete this task. To this end, a method of undetermined coefficients is presented to tackle this problem.

The rest of this paper is organized as follows. Firstly, the dynamical system under consideration is introduced in Section 2. In Section 3, the IHB algorithm is briefly introduced. The purpose of Section 4 is to deal with an obstacle arising in implementing the IHB method. And numerical examples and bifurcation analysis are presented in Section 5 and Section 6, respectively. This

paper ends with some remarks and conclusions in Section 7.

## 2. Dynamical system

The electrostatically actuated micro-cantilever in MEMS as shown in Fig. 1 is 4.5 um×80 um×200 um in dimensions (Liu *et al*. 2003). The motions of a cantilever beam should be inherently modeled by continuous theories of beam or plate. Although numerical simulations using such models can give accurate results when compared with experimental data (Homstein and Gottlieb 2008, Kacem *et al*. 2010), it is easier to understand the physics behind the nonlinear dynamic properties of electrostatic MEMS through a simpler mass-spring-damper model (De and Aluru 2006). The governing equation of motion for the micro-structure can be described as (Zhang and Meng 2005)

$$m\ddot{y}+c\dot{y}+ky=F_E(t_1) \tag{1}$$

where the superscript denotes the differentiation with respect to time $t_1$, $y$ the vertical displacement of the micro-cantilever relative to the origin of the fixed plate, $m$ the mass, $k$ and $c$ are the effective spring stiffness and damping coefficient of the simplified system, respectively. According to the parallel plate theory, the fringe effects at the edges of the plates are ignored (Price *et al*. 1989), hence $F_E$, the electrostatic force between the capacitor plates (the fixed plate and the movable plate) generated by applying a voltage $V(t)$, can be expressed by

$$F_E=\frac{\varepsilon_0 A}{2}\frac{V^2(t_1)}{(d-y)^2} \tag{2}$$

where $\varepsilon_0$ is the absolute dielectric constant of vacuum, $\varepsilon_0=8.5\times10^{-12}$ N/m, $A$ the overlapping area between the two plates, and $d$ is the gap between them. Other parameters are given as $m=3.5\times10^{-11}$ kg, $k=0.17$ N/m, $c=1.78\times10^{-6}$ kg/s, $A=1.6\times10^{-9}$ m$^2$ (Zhang and Meng 2005) and $d=1.2$ um.

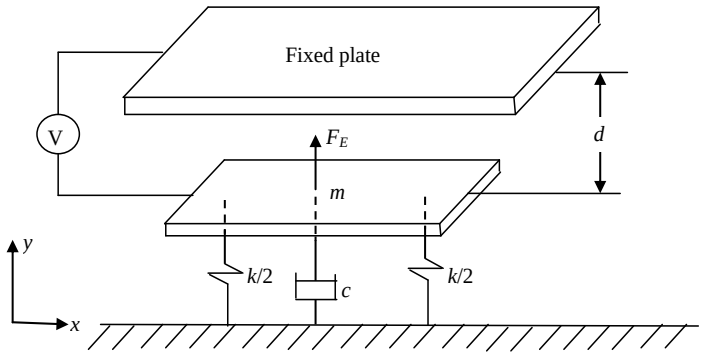


Fig. 1 A simplified dynamical model of the micro-cantilever in MEMS

Introducing the following dimensionless variables

$$x = y/d\ ,\quad \omega_0 = \sqrt{k/m}\ ,\quad t = \omega_0 t_1$$

then one can rewrite Eqs. (1) and (2) as

$$\ddot{x} + \zeta \dot{x} + x = T\frac{V^2(t)}{(1-x)^2} \tag{3}$$

where $\zeta = c/\sqrt{km}$, $T = \varepsilon_0 A/(2kd^3)$, and the superscript $(.)$ denotes the differentiation with respect to $t$. When the applied voltage, $V(t)$, includes alternating current (ac) voltage, $V_0\cos(\omega\tau)$, and polarization voltage, $V_P$, then one has $V(t) = V_P + V_0\cos(\omega t)$.

The inequity $x<1$ must hold because the movable plate is not allowed to contact the fixed one ($x$=1). Additionally, a mathematical singularity will arise for Eq. (3) if $x$ approaches 1. In such cases, the so-called pull-in happens. As we know, static and/or dynamic pull-in instability may arise in electrostatic actuated oscillators (Nayfeh et al 2007). The physically valid parameters should below the minimal escape threshold that leading to pull-in (Hassani *et al*. 2010). As Fig. 2 shows, there minimal values for both $V_p$ and $V_0$ above which dynamic pull-in may happen. Therefore, the parameters in this study are chosen below these minimal values according to Fig. 2.

In this study, $V_P = 0.5$ and $V_0 = 3$ are chosen, and $\omega$ is taken as a control parameter with varying value. Note that the fixed points of system (3) are $x = 0.1637$ and $x = 0.5392$, as plotted in Fig. 4. The first is stable whereas the latter unstable, according to stability theories for nonlinear dynamical systems.

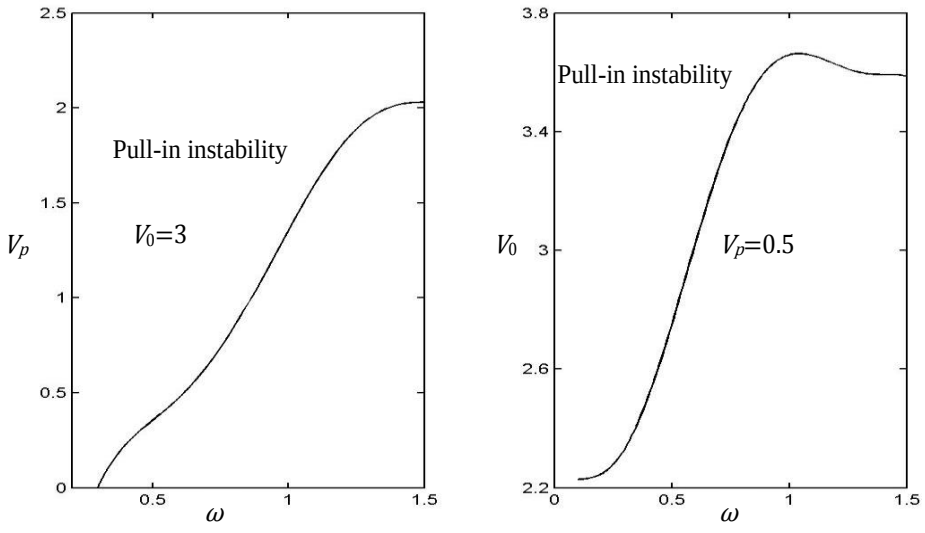


Fig. 2 The minimal values of voltage amplitudes above with dynamic pull-in instability happens

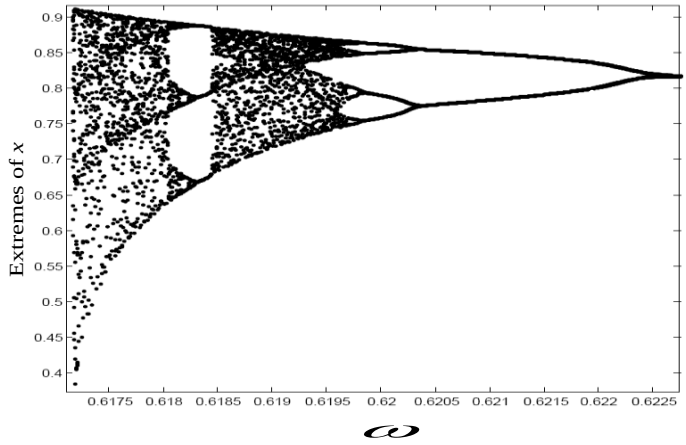


Fig. 3 Bifurcation chart of system (3) versus $\omega$

The bifurcation diagram of system (3) obtained by the Runge-Kutta method is presented in Fig. 3. There are two period doubling routes to chaos. One starts from a period-1 solution and the other from a period-3 solution. Usually, period doublings denote the evolution of a solution as the control parameter increasing. In our study, however, period doublings happen when the control parameter decreases. Sometimes, it is called as reversal period doubling bifurcation. For brevity, we call it period doubling.

In addition, as Fig. 3 shows, sub-harmonic responses arise intermittently even when the control parameter is located in a chaotic region. They constitute narrow periodic windows. Sub-harmonic solutions and period doublings are of fundamental interest of many researchers and engineers who are interested in nonlinear dynamics. For this issue, sub-harmonic responses will be intensively investigated in the following paper via the IHB method.

It is also worthy of pointing out that the displacement approaches closely 1 at the chaotic regions. In many electrostatic micro-oscillators, pull-in instability may exhibit when high level displacement happens. If the frequency decreases further, a dynamic pull-in will be confronted.

## 3. Incremental harmonic balance method

First of all, introduce a new time scale $\tau = \omega t / n$, where $\omega$ is the angular frequency of the electrostatic force, and *n* is introduced to seek a 1/*n* sub-harmonic response (or period-*n* solution). Eq. (3) becomes

$$\omega^2 x'' / n^2 + \zeta \omega x' / n + x - f(x, \tau) = 0 \tag{4}$$

where the nonlinear term $f(x,\tau) = T[V_p + V_0 \cos(n\tau)]^2 / (1-x)^2$.

The first step of the IHB method is a Newton-Raphson procedure. Let $x_i$ denote a state of vibration corresponding to $\omega = \omega_i$, the neighboring state can be expressed by adding the

corresponding increments to them as follows

$$x = x_i + \Delta x, \quad \omega = \omega_i + \Delta\omega \tag{5}$$

Substituting Eq. (5) into (4) and neglecting all the small terms of higher order, one obtains the following linearized incremental equation

$$\omega_i^2 \Delta x'' + \omega_i \zeta \Delta x' + (1 + \frac{\partial f(x_i, \tau)}{\partial x_i})\Delta x + (2\omega_i x_i'' + \zeta x')\Delta\omega + R(x_i, \omega_i, \tau) = 0 \tag{6}$$

where the residual

$R(x_i, \omega_i, \tau) = \omega^2 x_i'' / n^2 + \zeta\omega x_i' / n + x_i - f(x_i, \tau)$

goes to zero as $x_i$ approaches the exact solution of Eq. (3) with $\omega = \omega_i$.

The second step is the Ritz-Garlerkin procedure (Urabe 1965), let

$$x_i = \frac{1}{2}c_0 + \sum_{j=1}^{N}[c_j \cos(j\tau) + s_j \sin(j\tau)] \tag{7}$$

$$\Delta x = \frac{1}{2}\Delta c_0 + \sum_{j=1}^{N}[\Delta c_j \cos(j\tau) + \Delta s_j \sin(j\tau)] \tag{8}$$

Substituting Eqs. (7) and (8) into (6), and implementing the Garlerkin procedure results in a set of linear equations in terms of

$$\mathbf{K}_{\mathbf{u}}\Delta\mathbf{u} + \mathbf{K}_{\omega}\Delta\omega + \mathbf{K}_R = 0 \tag{9}$$

where $\Delta\mathbf{u} = [\Delta c_0, \Delta c_1, \Delta s_1, \cdots, \Delta c_N, \Delta s_N]^{\mathrm{T}}$, $\mathbf{K}_{\mathbf{u}}$ is the Jacobian square matrix of dimension $2N+1$, or called as the tangential stiffness matrix; $\mathbf{K}_{\omega}$ is the frequency gradient vector, and $\mathbf{K}_R$ is the residue vector. These matrixes and vectors depend upon the initial solutions $x_i$ and $\omega_i$. In the IHB method, usually, one parameter varying actively (called as the active increment) should be chosen to control the continuations of solutions. Provided that $\Delta\omega$ is given, Eq. (9) describes a set of equations in the increments $\Delta\mathbf{u}$ at each step, which can be solved iteratively. However, along an equilibrium path for varying $\omega$, it is possible that the solution curve may form a loop (when the Jacobian matrix $\mathbf{K}_{\mathbf{u}}$ is singular). In order to eliminate the singularity of $\mathbf{K}_{\mathbf{u}}$, one may use either the selective coefficient or the arc-length method (Leung and Fung 1990). The latter is chosen.

Introducing a path parameter $\eta$, one has an augmenting equation

$$g(\mathbf{u}, \omega) - \eta = 0 \tag{10}$$

The function $g(\mathbf{u}, \omega) = (\mathbf{u} - \mathbf{u}_i)^T(\mathbf{u} - \mathbf{u}_i) + (\omega - \omega_i)^2$ is a good choice, where $\mathbf{u}_i$ is constituted by the Fourier coefficients of $x_i$. Taking increments on $\mathbf{u}$, $\omega$ and $\eta$ in Eq. (10), respectively, one has

$$\frac{\partial g}{\partial \mathbf{u}^{\mathrm{T}}}\Delta\mathbf{u} + \frac{\partial g}{\partial \omega}\Delta\omega - \Delta\eta + g - \eta = 0 \tag{11}$$

Taking Eq. (9) into account, one constructs the augmented incremental equation

$$\begin{bmatrix} \mathbf{K}_u & \mathbf{K}_\omega \\ (\partial g/\partial \mathbf{u})^{\mathrm{T}} & \partial g/\partial \omega \end{bmatrix} \begin{bmatrix} \Delta \mathbf{u} \\ \Delta \omega \end{bmatrix} = -\begin{bmatrix} \mathbf{K}_R \\ g - \eta + \Delta \eta \end{bmatrix} \tag{12}$$

The arc-length parameter $\eta$ can be taken as the control parameter in constructing the solution curve with respect to varying $\omega$.

## 4. Fourier series expansion of fractional functions

Eq. (12) provides us with a purely linear iterative algorithm, through which semi-analytical solutions can be obtained. Notice that all the solution procedures are manipulated in the frequency-domain. Another problem arising in practicing consists in the difficulty in expanding the two fractional functions, i.e., $1/(1-x_i)^2$ in $\mathbf{K}_R$ and $1/(1-x_i)^3$ in Eq. (12) into truncated Fourier series. An omnipotence yet inefficient method of obtaining the Fourier coefficients is integrating the product in $\tau \in [0, 2\pi]$ of $1/(1-x_i)^2$ and each harmonic, i.e., $\cos(k\tau)$ and $\sin(k\tau)$. It is very cumbersome to do so, even though $x_i$ is given as a truncated Fourier series.

Denote the solution containing the *N*th-order harmonic that obtained in the nth iteration step

$$x_i = \sum_{j=0}^{N} [c_{i,j} \cos(j\tau) + s_{i,j} \sin(j\tau)] \tag{13}$$

where $N$ is a given positive integer denoting the highest harmonic. Substituting Eq. (13) into $I_i = 1/(1-x_i)^2$ or $I_i = 1/(1-x_i)^3$ and neglecting harmonics higher than the *N*th-order, one obtains

$$I_i = 1/\sum_{i=0}^{N} [\alpha_{i,j} \cos(j\tau) + \beta_{i,j} \sin(j\tau)] \tag{14}$$

where $\alpha_{i,j}$ and $\beta_{i,j}$ depend on $c_{i,j}$ and $s_{i,j}$, respectively. The problem is transformed into expanding the reciprocal of a truncated Fourier series as another one. In order to do so, assume the truncated Fourier series of $I_i$ as

$$I_i = \sum_{j=0}^{N} [\sigma_{i,j} \cos(j\tau) + \theta_{i,j} \sin(j\tau)] \tag{15}$$

where $\sigma_{i,j}$ and $\theta_{i,j}$ are unknowns to be determined. Substitution of Eq. (15) into the left side of Eq. (14) results in

$$\sum_{j=0}^{N} [\sigma_{i,j} \cos(j\tau) + \theta_{i,j} \sin(j\tau)] \times \sum_{j=0}^{N} [\alpha_{i,j} \cos(j\tau) + \beta_{i,j} \sin(j\tau)] = 1 \tag{16}$$

The left side of Eq. (16) can be also expanded into truncated Fourier series with *N* harmonics retained. The Fourier coefficients are in linear connection with $\sigma_{i,j}$ and $\theta_{i,j}$, respectively. Equating the Fourier coefficients of both sides to 0, one has

$$\mathbf{\Phi}\upsilon = e_1 \tag{17}$$

where $\upsilon = [\sigma_{i,0}, \sigma_{i,1}, \theta_{i,1}, \cdots, \sigma_{i,N}, \theta_{i,N}]^{\mathrm{T}}$ is the unknown vector of dimension $2\times N+1$, $e_1 = [1,0,\cdots,0]^{\mathrm{T}}$ is also a constant vector of dimension $2\times N+1$, and $\mathbf{\Phi}$ the coefficient matrix of dimension $(2\times N+1)\times(2\times N+1)$. Importantly, $\mathbf{\Phi}$ is only dependent upon $\alpha_{i,j}$ and $\beta_{i,j}$ but not upon $\upsilon$. Eq. (17) is a linear algebraic one, which governs the coefficients of the truncated Fourier series of $I_i$.

## 5. Sub-harmonic responses

As mentioned in Section 3, there are two period doubling routes to chaos. Figs. 3 and 4 show the evolution of the subharmonic response that bifurcates from a period-1 solution. One can observe that the phase curve of the period-1 solution evolutes into two cycles, two into four and four into eight, etc. The IHB solutions are in excellent agreement with the numerical results. Intuitively, a period solution that can be tracked by time marching integration is considered as stable. The basic shapes of these phases don't change too much as the period doubling proceeds. Also plotted in Fig. 4 are the fixed points of system (3), with both located within the phase planes.

Note that, tracking a higher periodic solution without losing accuracy needs more harmonics to be included. Otherwise, the accuracy will be lost. The period-2*n* solutions are tracked on the basis of the preceding period-*n* ones just before period doubling. The period-*n* solution is adopted as the initial guess when solving the period-2*n* one. The detailed procedures will be addressed in the next section. Note also that, the Runge-Kutta solutions are obtained by choosing the initial conditions for system (3) based on the IHB solutions.

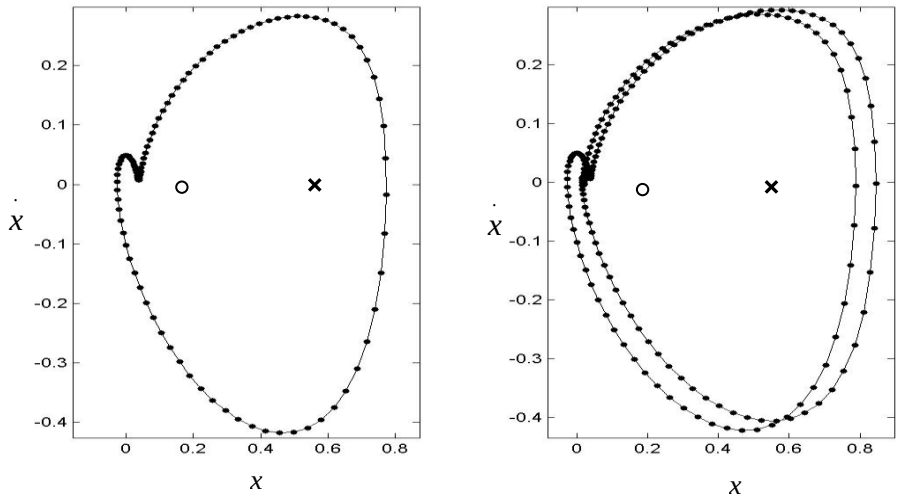


Fig. 4 Phase planes of period-1 ($\omega = 0.63$) and period-2 solutions ($\omega = 0.6213$). Solid lines denote the numerical results, and heavy dots the IHB solutions with *N*=32. The symbols "O" denote the stable fixed points, and "×" the unstable ones

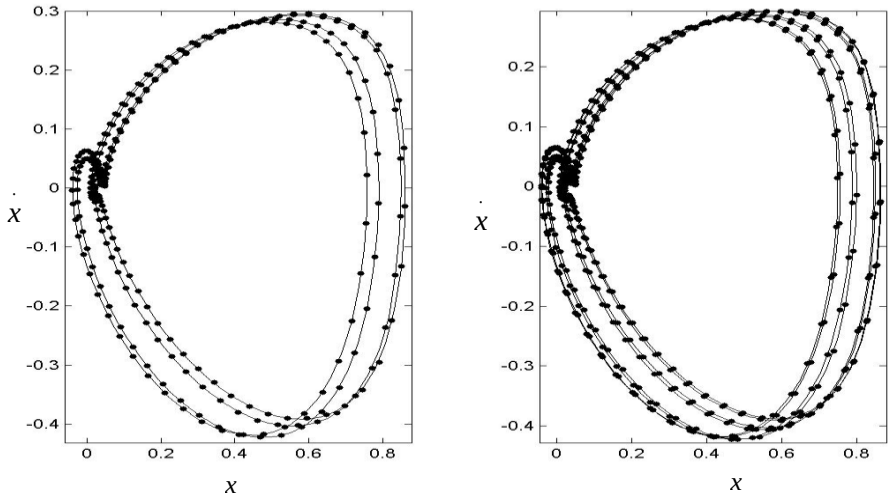


Fig. 5 Phase planes of period-4 ( $\omega = 0.62$ ) and period-8 solutions ( $\omega = 0.61976$ ). Solid lines denote the numerical results, and heavy dots the IHB solutions with *N*=96

Another period doubling bifurcation corresponds to the period-3 solution. As the control parameter $\omega$ decreases a little from 0.6183 to 0.6182, the period-3 solution evolutes to a period-6 one, shown in Fig. 6. As $\omega$ decreases further, the period of this solution doubles again, hence a period-12 solution arises (Fig. 7). Likewise, the basic shape of the periodic solution remains the same when the bifurcations arising. An FFT analysis was added to identify the frequency of the solution in Fig. 7 as shown in Fig. 8. The 1/12 frequency can be observed, though it is much smaller than the primary frequency.

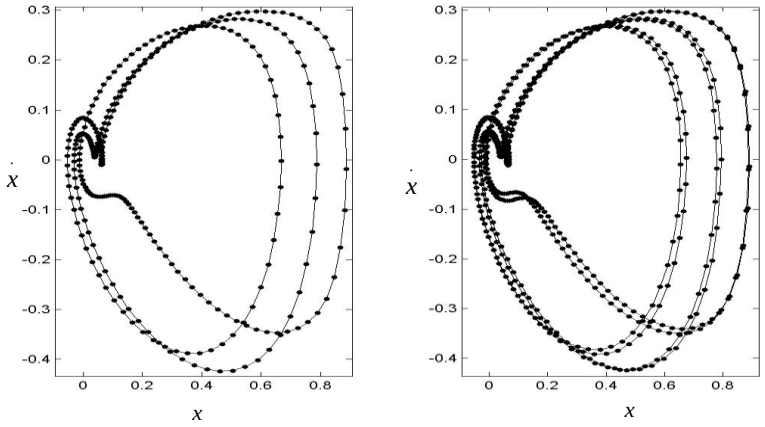


Fig. 6 Phase planes of period-3( $\omega = 0.6183$ ) and period-6 solutions ( $\omega = 0.6182$ ). Solid lines denote the numerical results, and heavy dots the IHB solutions with *N*=96

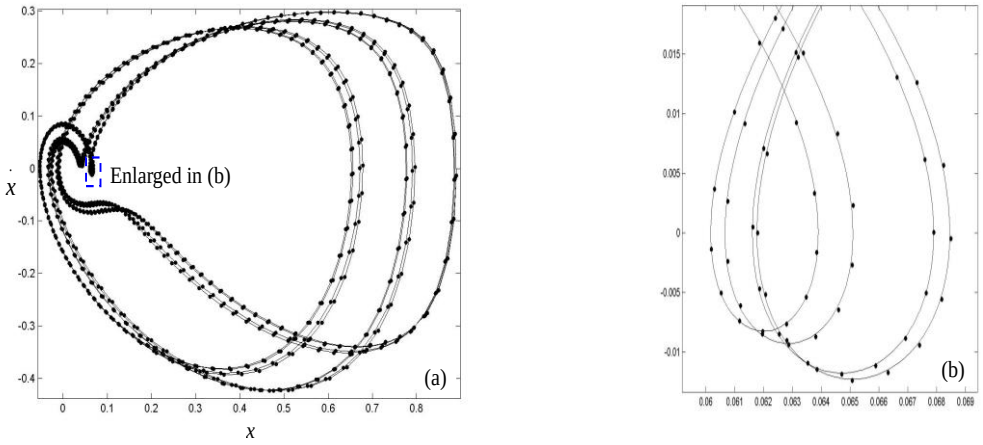


Fig. 7 Phase planes of period-12 ((a) with $\omega = 0.61818$ ) with an enlarged section (b). Solid lines denote the numerical results, and heavy dots the IHB solutions with $N$=240

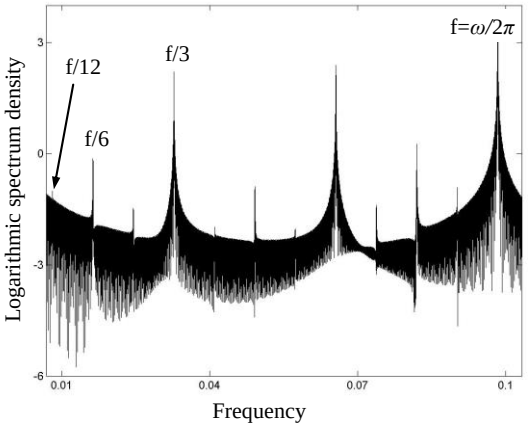


Fig. 8 The spectrum of time history shown in Fig. 6

Besides these sub-harmonic responses resulted from period doubling bifurcations, there are period-5 (Fig. 9) and period-7 (Fig. 11) solutions arising intermittently when the control parameter is in the chaotic region. Interestingly, the period-5 solution can also bifurcate into a period-10 one, as shown in Fig. 10. One can still clearly observe the nice agreement of the IHB solution with the numerical results from the enlarged part, though basically the period-10 solution is nearly the same as the period-5 one in configuration.

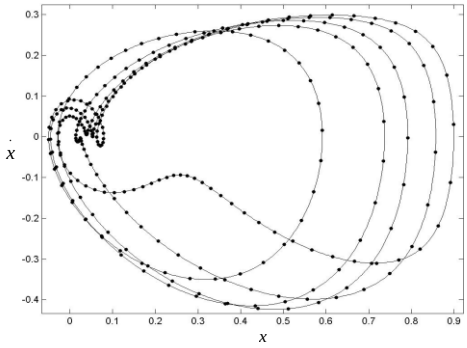


Fig. 9 Phase plane of a period-5 solution ( $\omega = 0.6177$ ). Solid line denotes the numerical results, and heavy dots the IHB solution with $N$=100

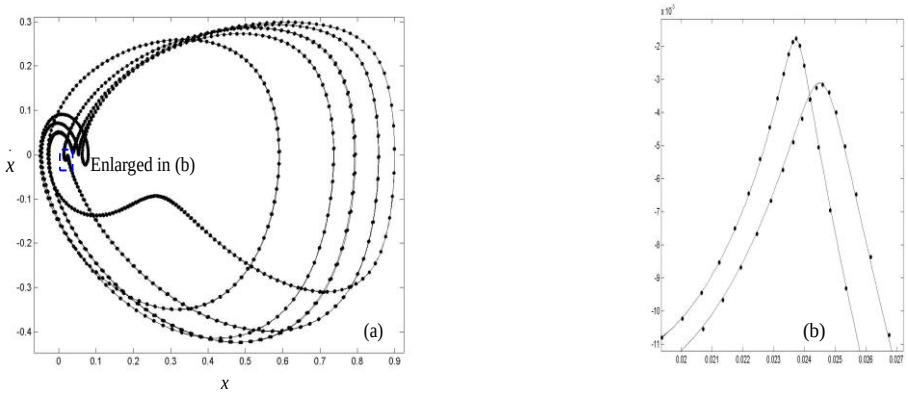


Fig. 10 Phase plane of a period-10 solution ((a) with $\omega = 0.61769$ ) and an enlarged section (b). Solid line denotes the numerical results, and heavy dots the IHB solution with $N$=200

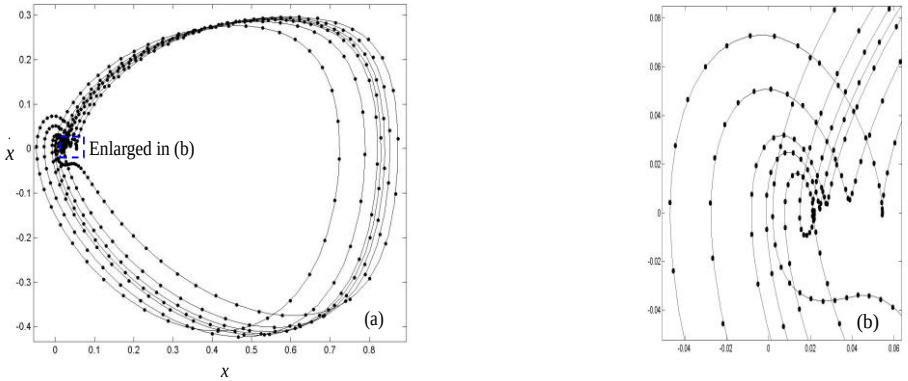


Fig. 11 Phase plane of a period-7 solution ((a) with $\omega = 0.619161$ ) and an enlarged section (b). Solid line denotes the numerical results, and heavy dots the IHB solution with $N$=100

## 6. Bifurcation analysis

As the two period doubling bifurcations proceed due to the decreasing of $\omega$, the periods of the solutions double step by step and finally approach infinity, then chaotic motions arise. Note that, the period doubling bifurcations happen when the control parameter is in a very small region. For instance, the route starting from the period-1 solution exists in $\omega \in [0.619, 0.6225]$ or so, and the one from period-3 solution arises in even narrower region, smaller than [0.6181, 0.6183]. Usually, a bifurcation point is determined by observing the phase plane and/or the Poincare map of a numerical solution, by letting the control parameter be a constant from time to time. In this section, we present an algorithm to find the period doubling bifurcation point more efficiently and accurately. This algorithm is based on the IHB method, as introduced above.

Fig. 4 demonstrates a fact that, the phase plane of the period-1 solution doesn't changes its shape after period doubling. The period-2 solution loses the 1/2 sub-harmonics. In other words, the coefficients of $\cos(\omega t/2)$ and $\sin(\omega t/2)$ converge to 0 when $\omega$ approaches the exact bifurcation point. Given a period-2*k* solution as

$$x^{2k} = \sum_{i=0}^{2N} [c_i^{2k} \cos(i\tau) + s_i^{2k} \sin(i\tau)] \tag{18}$$

As mentioned above, the non-dimensional time scale $\tau$ is defined as $\tau = \omega t/2k$. The superscript 2*k* denotes that *x* describes a period-2*k* solution. In the process that $x^{2k}$ evolutes as a period-*k* solution, the coefficients of the first harmonic (i.e., $c_i$ and $s_i$) approach 0. Under this assumption, one can let the coefficient of $\cos\tau$ in Eq. (7) be a very small quantity locating between 0 and $c_1^{2k}$, i.e.

$$c_1 = sign(c_1^{2k})\varepsilon \tag{19}$$

where $0 < \varepsilon << 1$. Note that $c_1$ remains the same in the IHB iteration algorithm, i.e., its incremental part $\Delta c_1$ is given as 0 and never changes. For every small quantity $\varepsilon$, there must be one period-2*k* solution for some value of $\omega$, which is dependent upon $\varepsilon$. Therefore, as $\varepsilon$ (or $c_1$) goes to 0, the 1/2*k* sub-harmonics eliminates and 1/*k* sub-harmonic become as the lowest one, which implies the convergent solution is of period-*k*. At the same time, $\omega$ converges to a constant. As long as enough harmonics are included, the limit of $\omega$ can converge very accurately to the exact bifurcation point where a period-*k* solution becomes a period-2*k* one. This bifurcation value is denoted by a bookkeeping parameter $\delta_k$.

Table 1 shows the convergence of $\delta_1$, $\delta_2$ and $\delta_3$ versus different values of $\varepsilon$. As one can see, the values of $\delta_k$ converge quickly to constants, respectively, as $\varepsilon$ decreases to 0. These constants are considered as approximate bifurcation values.

The Floquet theory is a powerful and routine technique to analyze the stability of periodic solutions. It points out that, a periodic solution is considered as stable when and only when all multipliers have absolute values less than 1 (Anishchenko 2002). When $\omega = \delta_3$, there exist two period solutions, i.e., a period-6 solution and a period-3 one. Notice that, there are two multipliers for every periodic solution of system (3). Notice also that, there is always one multiplier equaling to 0 for all the periodic solutions attained in this study. The non-zero Floquet multiplier

corresponding to the period-3 solution is -1.000018, while the one to the period-6 solution is 0.999985. If $\omega$ increases very a little, for instance, $\omega=\delta_3(1+10^{-9})$, the period-3 solution still exists and its Floquet multiplier is -0.999955. On the other hand, the period-6 solution disappears and becomes the period-3 one, that the coefficients of $c_{1,3,5,\ldots}$ and $s_{1,3,5,\ldots}$ converge to 0 simultaneously. As $\omega$ varies from $\delta_3(1+10^{-9})$ to $\delta_3$, therefore, the period-6 solution arises and the period-3 one loses its stability. This is a typical period doubling bifurcation. It is reasonable to say, the exact bifurcation value lies between $\delta_3$ and $\delta_3(1+10^{-9})$. Moreover, the relative discrepancy between $\delta_3$ and the exact bifurcation value is no more than $10^{-9}$, or $\delta_3$ is accurate to more than 9 decimal places.

According to the Feigenbaum theory (Feigenbaum 1978), as $n$ increases infinitely the space ratio of period-doubling bifurcation values, i.e., $\Delta_n=(\delta_n-\delta_{n-1})/(\delta_{n+1}-\delta_n)$ converges to the Feigenbaum constant (about 4.6692). Table 2 partly shows the numerical convergence of the space ratio to the constant as period-doubling bifurcations proceed. Note that 200 harmonics are included in the IHB algorithm when seeking these bifurcation values.

Table 1 Convergence of approximate bifurcation points versus coefficients of $\varepsilon$

| $\varepsilon$ | $\delta_1$, $N$=32 | $\delta_2$, $N$=100 | $\delta_3$, $N$=220 |
|---|---|---|---|
| 1e-4 | 0.62237470313040 | 0.62026540394587 | 0.61827516907512 |
| 1e-5 | 0.62237475492654 | 0.62026568071453 | 0.61827523043958 |
| 1e-6 | 0.62237475544450 | 0.62026568348224 | 0.61827523105322 |
| 1e-7 | 0.62237475544968 | 0.62026568350992 | 0.61827523105936 |
| 1e-8 | 0.62237475544973 | 0.62026568351020 | 0.61827523105942 |
| 1e-10 | 0.62237475544973 | 0.62026568351020 | 0.61827523105942 |

Table 2 Space ratios of period-doubling bifurcation values for system (3)

| $n$ | $\delta_n$ | $\Delta_n$ |
|---|---|---|
| 1 | 0.6223747 | |
| 2 | 0.6202657 | 4.700 |
| 4 | 0.619817 | 4.773 |
| 8 | 0.6197230 | 4.747 |
| 16 | 0.6197032 | 4.714 |
| 32 | 0.6196990 | |
| Feigenbaum constant | | 4.6692 |

Along the routes of period doublings, if increasing $\omega$ a little, system (3) gives rise up chaotic responses, as shown in Fig. 12 (figures (a) and (b)). The Poincare portraits of these responses are plotted in figure (b) and (d), respectively, where $T = 2\pi/\omega$ is the period of the nonlinear electrostatic force and $k = 1,2,3,\cdots$ . The chaos basins are similar to the chaotic solutions themselves in configuration.

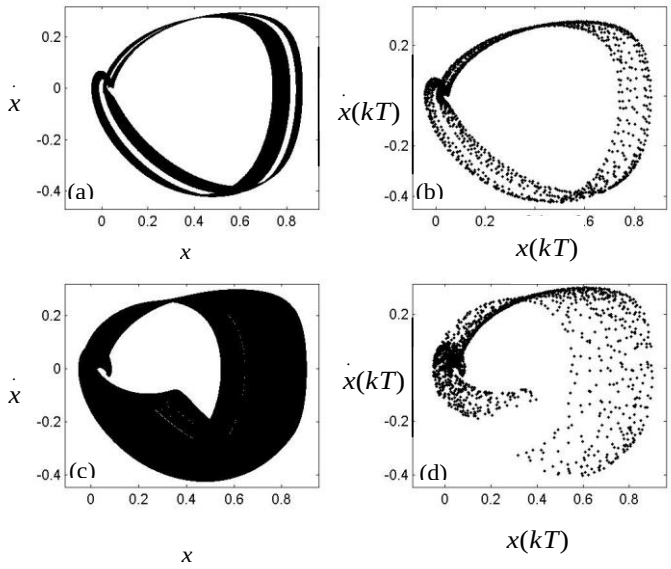


Fig. 12 Chaotic responses (a) ( $\omega = 0.6195$ ) and (c) ( $\omega = 0.618$ ) and their respective Poincare portraits (b) and (d)

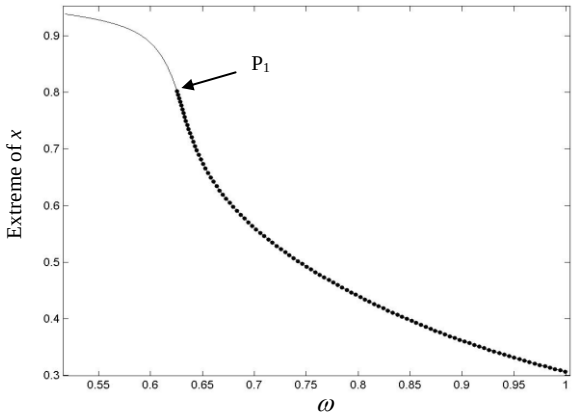


Fig. 13 The extreme values of period-1 solutions versus varying $\omega$, the heavy dots denote stable solutions while the solid line unstable one

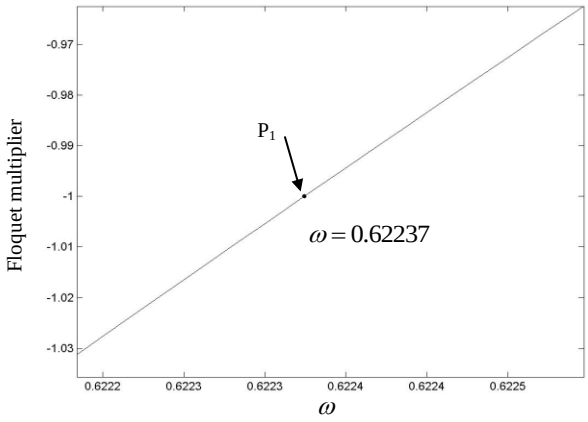


Fig. 14 The non-zero Floquet multiplier for parts of the period-1 solutions

Taking $\omega$ as a control parameter, the bifurcation chart of the period-1 solutions is presented in Fig. 13, also attained by the IHB method. Note that only the extreme values of the solutions are presented. As $\omega = 1$ decreases, the extreme values increases monotonously. The stability is also judged by computing the Floquet multipliers. Figs. 13 and 14 show that, when $\omega$ increases beyond about 0.62237, the non-zero multiplier decreases beyond -1 from a value larger than -1, which means a period doubling happens at point $P_1$. After $P_1$, the period-1 solution still exists, however it becomes unstable according to the Floquet theory.

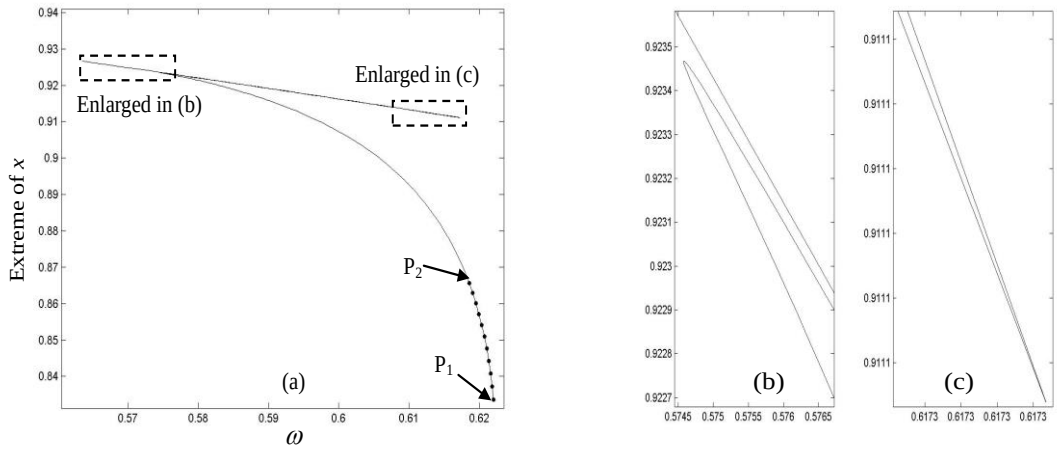


Fig. 15 The extreme values of period-2 solutions versus varying $\omega$, the heavy dots denote stable solutions while the solid line unstable one

More importantly, a period-2 solution arises just at P1, as shown in Fig. 15. According to Fig. 16, the non-zero Floquet multiplier for the period-2 solution decreases from 1. As $\omega$ decreases further, the absolute value of the Floquet multiplier remains less than 1 until $\omega$ gets a value of 0.62027. This value is denoted by the point $P_2$ in Figs. 15 and 16. At $P_2$, the multiplier passes through -1, which means the period-2 solution bifurcates as a period-4 one. After P2, likewise, the period-2 solution becomes unstable though it still exists, with a multiplier smaller than -1.

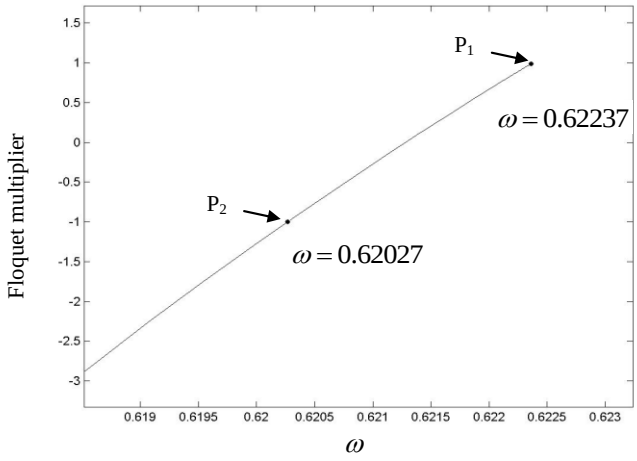


Fig. 16 The non-zero Floquet multiplier corresponding to parts of the period-2 solutions

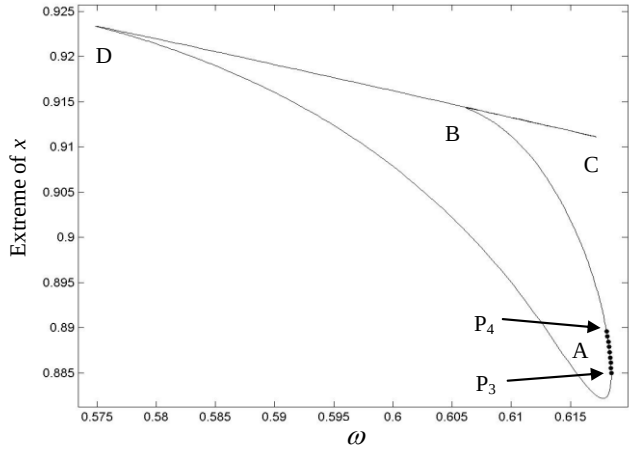


Fig. 17 The extreme values of period-3 solutions versus varying $\omega$, the heavy dots denote stable solutions while the solid line unstable one

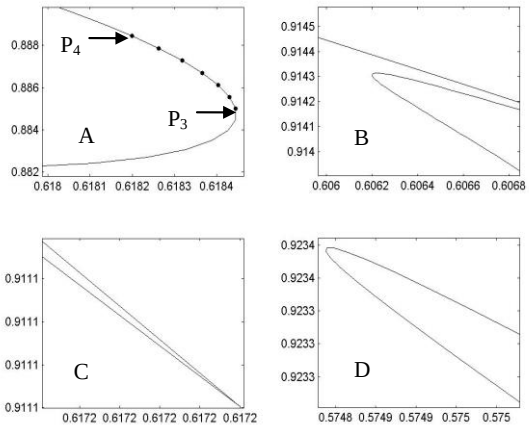


Fig. 18 Four enlarged parts of Fig. 15

The bifurcation chart of the period-3 solution is presented in Fig. 17, with four enlarged parts plotted in Fig. 18. Different from the period-1 and period-2 solutions, the period-3 solutions constitute a closed curve. Though it exists in a relatively broad area, about $\omega \in [0.575,0.625]$, it is only stable in a very narrow region, i.e., from $P_3$ to $P_4$. As $\omega$ decreases through $P_3$, two period-3 solution arise. One is stable and the other unstable. Along the lower part of the curve plotted in Fig. 18 (a), the multiplier decreases from more than 1 and passes 1 at point $P_3$, shown in the upper curve of Fig. 19. Then, the solution gains its stability between $P_3$ and $P_4$. At the same time, the multiplier decreases from 1 at $P_3$ to -1 at $P_4$. Similarly to the cases of the period-1 and the period-2 solutions, a period doubling exists at $P_4$. At this point, the period-3 solution becomes unstable and a stable period-6 solution arises.

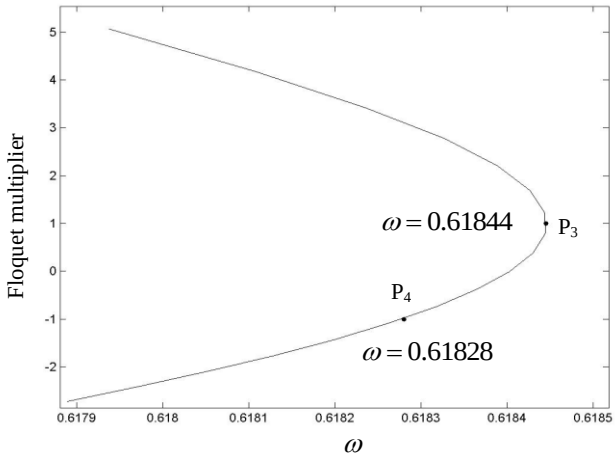


Fig. 19 Parts of Floquet multipliers corresponding to period-3 solutions

The effects of the voltages on the bifurcations are discussed briefly, with $\omega = 0.621$ as an illustration. Figs. 20 and 21 show the period doublings when voltage amplitudes $V_P$ and $V_0$ sweep, respectively. The period doubles in very narrow regions such that the distances from period-1 solution to period-8 one are at the order of $10^{-3}$ for both $V_P$ and $V_0$. In addition, the period doublings will lead to chaos if $V_P$ (or $V_0$) increases a little. Moreover, dynamic pull-in stability will arise soon after chaos if the voltages increase further.

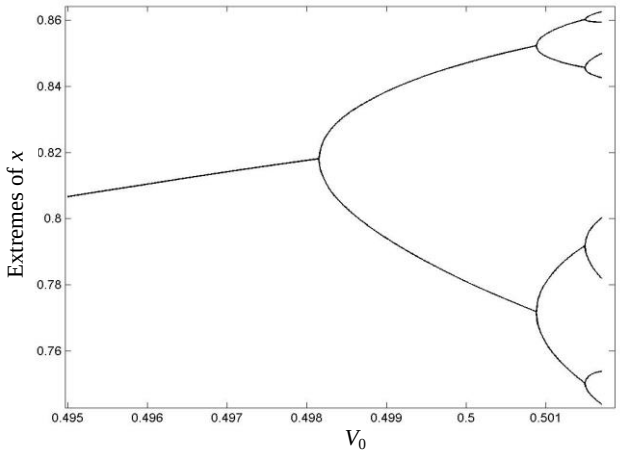


Fig. 20 The bifurcation chart versus $V_p$ obtained by the IHB with $N$=64, $\omega = 0.621$ and $V_0 = 3$

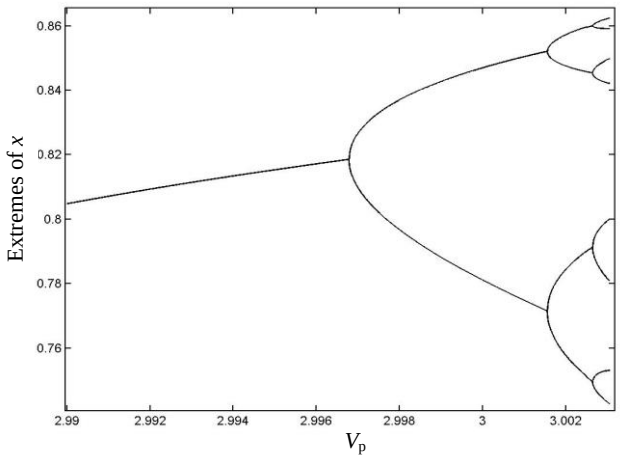


Fig. 21 The bifurcation chart versus $V_p$ obtained by the IHB with $N$=64, $\omega = 0.621$ and $V_P = 0.5$.

## 7. Conclusions

The incremental harmonic balance method has been employed to analyze the bifurcation of the nonlinear dynamical system of an electro-statically actuated micro-cantilever. During the solution procedure, an inevitable difficulty is confronted when expanding the nonlinear terms as truncated Fourier series. A coefficient undetermined approach is proposed to tackle this problem. With the help of this technique, very high harmonics can be included in the IHB algorithm. This guarantees the excellent agreement of the IHB solutions with the numerical results. Moreover, the IHB can be used to seek both stable and unstable solutions.

It is found that when altering the angular frequency of the electrostatic force, many sub-harmonic responses can arise. Some of those solutions are resulted from period doubling bifurcation, for example the period-2, 4, 8 solutions that from period-1 one, and the period-6 and period-12 solutions stemming from period-3, both in manner of period doublings. There are also period-5 and period-7 solutions arising intermittently even when the system exhibits chaotic responses. Interestingly, though the period-5 solution exists in a rather small parametric region, they can also bifurcate via period doubling. Additionally, the bifurcation diagrams of the period-1, period-2 and period-3 are analyzed, respectively, with the help of the presented algorithms and the Floquet theory. They all bifurcate in manner of period doubling, accompanied by the typical phenomenon that the non-zero Floquet multipliers decrease through -1.

In addition, a means for determining a period doubling point is introduced. This method makes it efficient to determine the bifurcation point with high precision. The IHB method, together with the undetermined coefficient method for Fourier series expansion as well as the approach for determining bifurcation value, could be applicable in more nonlinear dynamical systems, especially those with nonlinear terms expressed as fractional functions.

## Acknowledgements

This work is supported by NSFC (11002088, 11172333, and 11272361), and Natural Science Foundation of Guangdong Province (S2012040007920).

## References

Anishchenko, V.S., Astakhov, V.V., Neiman, A.B. *et al*. (2002), *Nonlinear dynamics of chaotic and stochastic systems*, Springer-Verlag Berlin Heidelberg.

Ashhab, M., Salapaka, M.V., Dahleh, M. and Mezic, I. (1999), "Dynamic analysis and control of microcantilevers", *Automatica*, **35**, 1663-1670.

Bayat, M. and Pakar, I. (2012), "Accurate analytical solution for nonlinear free vibration of beams", *Struct. Eng. Mech.*, **43**(3), 337-347.

Borzi, B., Vona, M., Masi, A. *et al*. (2013), "Seismic demand estimation of RC frame buildings based on simplified and nonlinear dynamic analyses", *Eartq. Struct*., **4**(2).

Chan, E.K. and Dutton, R.W. (2000), "Electrostatic micromechanical actuator with extended range of travel", *J. Microelectromech. S.*, **9**(3), 321-328.

Chen, Y.M., Meng, G. and Liu, J.K. (2010), "An iterative method for nonlinear dynamical system of an electrostatically actuated micro-cantilver", *Phys. Lett. A*, **374**, 3455-3459.

De, S.K. and Aluru, N.R. (2006), "Complex nonlinear oscillations in electrostatically actuated

microstructures", *J. Microelectromech. S.*, **15**(2), 355-369.
Feigenbaum, M. (1978), "Qualitative universality for a chaos of nonlinear transformations", *T. Stat. Phys.*, **19**, 5-32.
Ferri, A.A. (1986), "On the equivalence of the incremental harmonic balance method and the harmonic balance-Newton Raphson method", *J. Appl. Mech, - ASME*, **53**, 455-457.
Fu, Y.M. and Zhang, J. (2009), "Nonlinear static and dynamic response of an electrically actuated viscoelastic microbeam", *Acta Mech. Sinca*, **25**(2), 211-218.
Hassani, F.A., Payam, A.F. and Fathipour, M. (2010), "Design of a smart MEMS accelerometer using nonlinear control principles", *Smart Struct. Syst.*, **6**(1), 1-16.
Hornstein, S. and Gottlieb, O. (2008), "Nonlinear dynamics, stability and control of the scan process in noncontacting atomic force microscopy", *Nonlinear Dynam.*, **54**, 93-122.
Hu, S.Q. and Raman, A. (2006), "Chaos in atomic force microscopy", *Phys. Rev. Lett.*, **96**, 036107.
Kacem, N., Arcamone, J., Perez-Murano, F. and Hentz, S. (2010), "Dynamic range enhancement of nonlinear nanomechanical resonant cantilever for highly sensitive NEMS gas/mass sensor applications", *J. Micromech. Microeng.*, **20**(4), 1-9, 045023.
Lau, S.L. and Cheung, Y.K. (1981), "Amplitude incremental variational principle for nonlinear vibration of elastic systems", *J. Appl. Mech. - ASME*, **48**(4), 959-964.
Leung, A.Y.T. and Fung, T.C. (1990), "Construction of chaotic regions", *J. Sound Vib.*, **131**(3), 445-455.
Liu, S., Davidson, A. and Liu, Q. (2003), "Simulating nonlinear dynamics and chaos in a MEMS cantilever using Poincare mapping", *Proceedings of the IEEE, Transducers'03, the 12th International Conference on Solid State* Sensors *Actuators and Microsystem*s, Boston, 8-12 June.
Liu, S., Davidson, A. and Liu, Q. (2004), "Simulation studies on nonlinear dynamics and chaos in a MEMS cantilever control system", *J. Micromech. Microeng.*, **14**(7), 1064-1073.
Lyshevski, S.E. (1997), "Nonlinear microelectromechanic systems (MEMS) analysis and design via the Lyapunov stability theory", *Proceeding of the 40th IEEE Conference on Decision and Control Orlando*, FL USA.
Mahmoodi, S.N. and Jalili, N. (2009), "Piezoelectrically actuated microcantilevers: An experimental nonlinear vibration analysis", *Sens. Actuat. A*, **150**(1), 131-136.
Manna, M.C., Bhattacharyya, R. and Sheikh, A.H. (2010), "Nonlinear dynamic response and its control of rubber components with piezoelectric patches/layers using finite element method", *Smart Struct. Syst.*, **6**(8), 89-903.
Meng, G., Zhang, W.M., Huang, H., Li, H.G. and Chen, D. (2009), "Micro-rotor dynamics for micro-electro-mechanical systems (MEMS)", *Chaos Soliton. Fract.*, **40**(2), 538-562.
Najar, F., Nayfeh, A.H., Abdel-Rahman, E.M., Choura, S. and El-Borgi, S. (2010a), "Nonlinear analysis of MEMS electrostatic microactuators: primary and secondary resonances of the first mode", *J. Vib. Control*, **16**(9), 13-21.
Najar, F., Nayfeh, A.H., Abdel-Rahman, E.M., Choura, S. and El-Borgi, S. (2010b), "Dynamics and global stability of beam-based electrostatic microactuators", *J. Vib. Control*, **16**(5), 721-748.
Nayfeh, A.H. and Younis, M.I. (2005), "Dynamics of MEMS resonators under superharmonic and subharmonic excitations," *J. Micromech. Microeng.*, **15**(10), 1840-1847.
Nayfeh, A.H., Younis, M.I. and Abdel-Rahman, E.M. (2007), "Dynamic pull-in phenomenon in MEMS resonators", *Nonlinear Dynam.*, **48**(1-2), 153-163.
Passiana, A., Muralidharana, G., Mehtaa, A., Simpson, H., Ferrell, T.L. and Thundat, T. (2003), "Manipulation of microcantilever oscillations", *Ultramicroscopy*, **97**(1-4), 391-399.
Price, R.H., Wood, J.E. and Jacobsen, S.C. (1989), "Modeling considerations for electrostatic forces in electrostatic microactuators", *Sensor. Actuat. A*, **20**(1-2), 107-114.
Raghothama, A. and Narayanan, S. (1999), "Non-linear dynamics of a two-dimensional airfoil by incremental harmonic balance method", *J. Sound Vib.*, **226**(3), 493-517.
Senturia, S.D. (1998), "Simulation and design of microsystems: a 10-year preserve", *Sens. Actuat. A*, **67**, 1-7.
Shen, J.H., Lin, K.C., Chen, S.H. and Sze, K.Y. (2008), "Bifurcation and route-to-chaos analyses for

Mathieu-Duffing oscillator by the incremental harmonic balance method", *Nonlinear Dynam*., **52**(4), 403-414.
Towfighian, S., Hppler, G.R. and Abdel-Rhman, E.M. (2011), "Analysis of a chaotic electrostatic micro-oscillator", *J. Comput. Nonlinear Dyn*., **6**(1), 1-10, 011001
Urabe. M. (1965) "Galerkin's procedure for nonlinear periodic systems", *Arch. Ration. Mech. An.*, **20**(2), 120-152.
Waris, M.B. and Ishihara, T. (2012), "Dynamic response analysis of floating offshore wind turbine with different types of heave plates and mooring systems by using a fully nonlinear model", *Coupled Syst. Mech*., **1**(3), 247-268.
Xu, L., Lu, M.W. and Cao, Q. (2003) "Bifurcation and chaos of a harmonically excited oscillator with both stiffness and viscous damping piecewise nonlinearities by incremental harmonic balance method", *J. Sound Vib.*, **264**(4), 873-882.
Zhang, W.M. and Meng, G. (2005), "Nonlinear dynamical system of micro-cantilever under combined parametric and forcing excitations in MEMS", *Sens. Actuat. A*, **119**(2), 291-299.
Zhang, W.M., Meng, G. and Chen, D. (2007), "Stability, nonlinearity and reliability of electrostatically actuated MEMS devices", *Sensors*, **7**, 760-796.

*CC*